THE SOLAR NEUTRAL IRON SPECTRUM

I: *Measurement of Solar Fe I Line Profiles from Center to Limb*

BRUCE W. LITES

High Altitude Observatory, National Center for Atmospheric Research, Boulder, Colo., U.S.A.*

and

J. W. BRAULT

Kitt Peak National Observatory, Tucson, Ariz., U.S.A.*

(Received 26 February, 1973)

Abstract. Mean profiles of eighteen neutral iron lines of varying strengths were measured at selected positions from the center of the solar disk to the limb. These profiles were obtained by rapid photoelectric scanning of the spectrum with a double-pass spectrometer. The Fe I lines selected are representative of most of the stronger low-lying transitions in the neutral iron atom. In addition to the iron lines, this observational program includes center-to-limb measurements of three Ti II lines and of the Ca I resonance line λ4226.7. The line profiles are presented here in graphical form after correction for instrumental effects and normalization to the local disk center continuum.

1. Introduction

The presence of numerous strong neutral iron lines in the solar spectrum suggests that Fe I contributes significantly to the total solar line blanketing. These lines also exhibit several marked center-to-limb characteristics (Athay *et al.*, 1972) that give insight into the general formation of spectral lines in the solar atmosphere, and the large range of the strength of the neutral iron lines suggests that the detailed study of their formation processes will yield information on the structure of the solar atmosphere. For these reasons alone the neutral iron lines play a significant role in the study of the solar atmosphere, but the analysis of these strong lines has been deferred until very recently (Tanaka, 1971a, b) because of the complexity of the neutral iron atomic structure. We undertake the analysis of the solar neutral iron spectrum using line profile synthesis. Heretofore, however, no measurements of these line profiles have been made which are of the quality necessary for this type of analysis. In this paper we describe the measurement and subsequent numerical processing of mean solar profiles of eighteen representative neutral iron lines (and, in addition, three lines of Ti II and the Ca I resonance line λ4226.7) at selected positions from the center of the disk to the limb, and we defer description of the details and results of the Fe I line profile synthesis to a following paper.

The intended use of these observed profiles for comparison with synthesized profiles imposes some requirements upon the nature and quality of the observed data. Among these requirements are (1) high resolution of the profiles in wavelength, (2) a certain

* Both Kitt Peak National Observatory and the National Center for Atmospheric Research are sponsored by the National Science Foundation.

Solar Physics **30** (1973) 283–300.

(but rather ill-defined) minimum sampling of the profiles across the disk, (3) the ability to effect an absolute intensity calibration on the profiles at all disk positions, and (4) a reliability of the observed intensities exceeding the accuracies involved in the theoretical treatment. Attainment of these requirements is limited by some practical observational problems. Among the most important of these are: (1) seeing effects, (2) noise present in the data from the measurement process, (3) instrumental wavelength resolution, and (4) the availability telescope observing time. Much of this paper is devoted to a brief description of the observational and numerical methods used to minimize the effect of these problems. A more complete discussion of the details of these procedures can be found in Lites' thesis (Lites, 1972).

In Section 2 we describe the measurement of the basic profile data, and in Section 3 we discuss the auxiliary measurements necessary to correct the data for systematic instrumental effect and calibrate the data to an absolute intensity scale. Section 4 is a summary of the numerical processing procedure for the data, and in Section 5 the quality of the measurements and sources of error remaining in the processed data are discussed. In Section 6 the data is presented in graphical form.

2. The Line Profile Data

The following four criteria were used as guidelines in selection of the Fe I lines to be observed.

(a) One of the principal objectives of the study of the solar neutral iron spectrum is the investigation of chromospheric conditions at the heights where the strong neutral iron lines are formed. The set of observed lines should therefore include a sampling of the stronger Fe I lines in the solar spectrum.

(b) Several weaker lines should also be included in the set of observed lines. These weaker lines are useful in the investigation of the atmosphere between the middle photosphere ($\tau_{5000} \sim 10^{-1}$) and the formation region of the strong lines.

(c) The selected lines must include transitions representative of the multiplets that are important to the ionization and excitation equilibrium of Fe I at the heights in the solar atmosphere where departures from LTE in iron are important.

(d) The line profiles, especially the line cores, must be relatively free of blends.

As a result of these four criteria the selection of lines weights heavily the strong low lying multiplets of Fe I. In general, the strongest apparently unblended line within each selected multiplet was chosen for observation. Table I indicates the scope of the observing program. Listed in the first two columns of this table are the wavelengths of the observed lines and the respective observed disk positions, or μ-positions. Note that most of the observations occur in the wavelength range 3500 Å to 4500 Å.

The acquisition of mean high dispersion spectra of the chosen neutral iron absorption lines was carried out at Kitt Peak National Observatory from May to August, 1970. In this program we used the 84-in. McMath Solar Telescope and the fast scan grating spectrometer in the double-pass mode to obtain photoelectric scans several ångströms long at selected positions across the disk. Brault *et al.* (1971) describe the operation of

the McMath Solar Telescope, the spectrometer, and the data recording system when used in acquisition of spectra of the type obtained here. The raw profile data are the averages of many measurements of the photometer voltage, which was sampled at intervals of a few milli-ångströms. The basic profile data then provides only relative intensities within the wavelength range of each scan.

The observing procedure used to obtain the basic profile data is essentially the same as the spectrum scanning procedure described by Brault *et al.* (1971), so here we indicate only the specific settings of the spectrometer and telescope necessary to obtain the mean profiles at the selected μ-positions. Henceforth the basic data scans are referred to as 'profile scans'.

The third and fourth columns of Table I list respectively the spectrometer grating order and the type of broadband order isolating filter used for each observed line. All of the profile scans are 2048 grating rotation steps long. The three slits (S_1, S_2, S_3) had respective openings of 100, 160, and 100 μ. All spectrum scans were taken with the ITT FW130 photomultiplier with an S-20 photocathode.

Each profile scan required 20 min of telescope time, however the actual integration time is less than 10 min because of the scattered light measurement on each return scan of the grating as described by Brault *et al.* and because of the inter-scan dead time. A profile measurement is then the average of 172 individual scans.

The limb guiders maintained the image position relative to the spectrometer slit. All μ-positions were measured from the geocentric north limb of the Sun. We used a quartz image integrating lens for profiles obtained at the center of the disk only.

The seeing conditions and time of day dictate the optimum use of the spectrometer. Atmospheric extinction increases rapidly with both zenith angle and photon frequency; hence, the profile scans of the lines at the shorter wavelengths were obtained near-noon for best signal-to-noise ratios. The best daytime seeing during the summer months (at Kitt Peak) generally occurs during the second and third hours after sunrise, so these periods were reserved, if the seeing was indeed good, for profile scans of the most extreme limb positions ($\mu=\frac{1}{7}$ to $\mu=\frac{1}{10}$).

Although no Hα patrol data was available on a daily basis to discern regions of chromospheric activity, we avoided taking data in obvious active regions, determined by the presence of sunspots, during measurement of line profiles.

3. The Auxiliary Measurements

The auxiliary measurements may be separated into two classes: (1) those necessary for calibration of the profile scans to an absolute intensity scale, (2) those used in correction of systematic instrumental effects.

Adjustments of the profile scans to an absolute intensity scale requires at minimum a knowledge of the relative intensities at the selected μ-positions at some wavelength included in all scans of a line, and a knowledge of the absolute intensity at some wavelength in one scan of the line. The first auxiliary measurement is then the direct measurement of the limb darkening function at a specific wavelength

TAB

Scope of the observing pro

Line λ	Observed μ-position 1 $^2/_3$ $^1/_2$ $^1/_3$ $^1/_4$ $^1/_5$ $^1/_6$ $^1/_7$ $^1/_8$ $^1/_9$ $^1/_{10}$	Grating order	Corning glass filter	Drift scan wavelength λ
Fe I				
3440.626	× × × × × × ×	8	7–54	3439.428
3608.869	× × × × × × ×	8	7–54	3607.275
3719.947	× × × × × × × × × × ×	7	5–57	3718.537
3734.874	× × × × × × × × × × ×	7	5–57	3736.134
3815.851	× × × × × × ×	7	5–57	3817.189
3820.436	× × × × × × × × × × ×	7	5–57	3818.916
3886.294	× × × × × × × × × × ×	7	5–57	3883.924
4063.605	× × × × × × ×	7	5–57	4064.847
4271.774	× × × × × × × × × × ×	6	5–56	4272.720
4383.557	× × × × × × × × × ×	6	5–56	4382.340
4404.761	× × × × × × × × × × ×	6	5–56	4406.382
4415.135	× × × × × × × × × × ×	6	5–56	4417.106
4602.949	× × × × × × ×	6	5–56	4604.847
5123.730	× × × × ×	5	4–97	5122.624
5198.718	× ×	5	4–97	5196.852
5227.192	× ×	5	4–97	5228.987
5269.550	× × × × × ×	5	4–97	5267.903
6430.856	× × × ×	4	3–69	6429.011
Ti II				
3641.335	× × × × ×	8	7–54	3640.830
3685.196	× × ×	7	5–57	3683.794
3913.470	× × × × × × ×	7	5–57	3913.877
Ca I				
4226.740	× × × × × × ×	6	5–56	4228.892

[a] DS means drift scan data, the measurement as described in text; PW means Pierce and Waddell (1961) darkening data.
[b] Drift scan data found for 3818.916 were used for this line.
[c] H means Houtgast (1970); LN means Labs and Neckel (1968).

included in all the profile scans of a line. Henceforth we label these meaments *drift scans*. Absolute intensity measurements are beyond the scope of this observational program, so (a) we adopt the monochromatic disk center absolute intensities at the *continuum windows* given by Houtgast (1970) below 4100 Å, and (b) above 4100 Å we adopt the disk center continuum intensities inferred by Labs and Neckel (1968) from their broadband absolute intensity measurements. The appropriate continuum window of Houtgast (1970) or a suitable point of application of the Labs and Neckel (1968) intensities generally does not occur within the wavelength range of the profile scans. In order to calibrate the relative profile intensities to the absolute measurements of the sources (a) and (b) *long scans* were made at the center of the disk. The long scans are the second type of auxiliary measurement. They span the wavelength range of the profile scan and include one or more wavelengths where the absolute intensity is given by the above-mentioned authors.

; scan	Type of limb darkening calibration[a]	'Continuum window' wavelength λ	Intensity of continuum window (10^{14} erg/cm^2 ster s $\Delta\lambda = 1$ cm)	Source of absolute intensity data[c]
-3451	DS	3439.400	2.51	H
-3617	DS	3607.200	2.95	H
-3730	DS	3715.000	3.37	H
-3743	DS	3729.200	3.37	H
-3826	DS[b]	3811.500	3.91	H
-3834	DS	3828.700	2.28	H
-3888	DS	3883.900	3.59	H
-4071	DS	4061.300	4.22	H
-4284	DS	4279.287	4.59	LN
-4399	DS	4394.452	4.68	LN
-4414	DS	4401.979	4.39	LN
-4426	DS	4409.752	4.56	LN
-4612	PW	4601.710	4.36	LN
-5136	PW	5130.790	4.05	LN
-5210	PW	5196.852	3.89	LN
-5238	PW	5228.984	3.93	LN
-5280	DS	5261.124	3.95	LN
-6446	PW	6429.008	2.98	LN
-3647	PW	3640.799		
-3694	PW	3681.397		
-3931	DS	3911.499		
-4237	DS	4230.787	4.73	LN

It is possible to measure some of the systematic errors present in the raw profile scans so that the effects of these errors may be subsequently removed during the numerical processing. The third auxiliary measurement indicates the magnitude of one such error: the slow variation of the spectrometer response with wavelength. We call this type of auxiliary measurement a *standard lamp scan* since spectrum scans of a light source having a known dependence of emitted energy with wavelength were obtained. Brault *et al.* (1971) have measured the finite wavelength resolution of the spectrometer in the form of an instrumental response profile. This instrumental profile constitutes the fourth auxiliary measurement. We do not consider further the measurement of the instrumental profile since this has already been done adequately by Brault *et al.* (1971).

A. THE DRIFT SCANS: MEASUREMENT OF THE LIMB DARKENING FUNCTION

In order to establish a relative intensity scale for spectrum scans at different μ-positions,

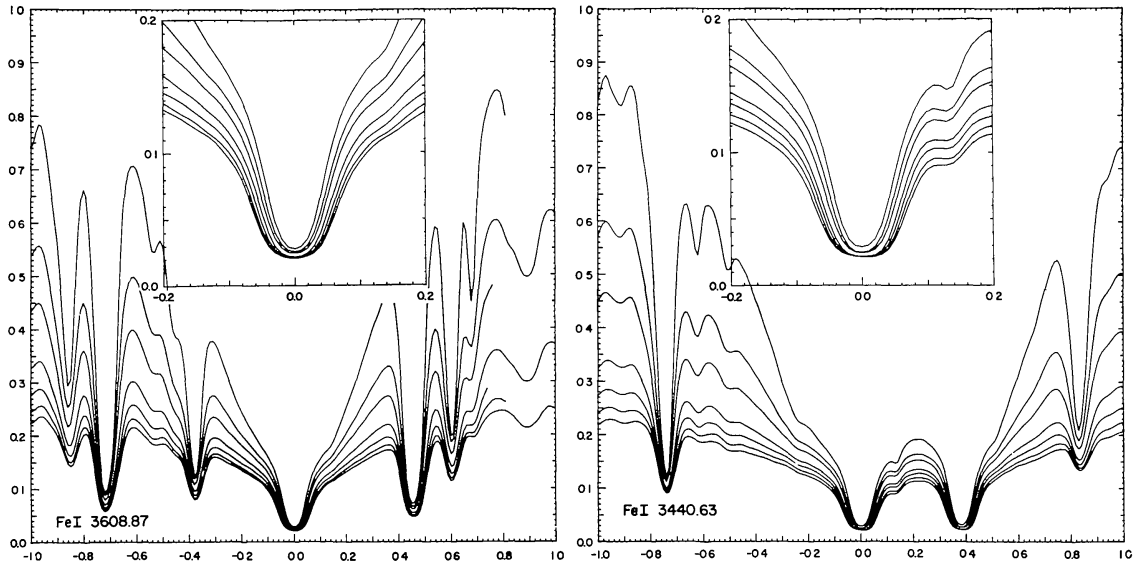

Fig. 1a. The limb darkening in the line profiles of Fe I 3608.87 and Fe I 3440.63. Refer to Table I for the values of $\mu = \cos\theta$ for each profile.

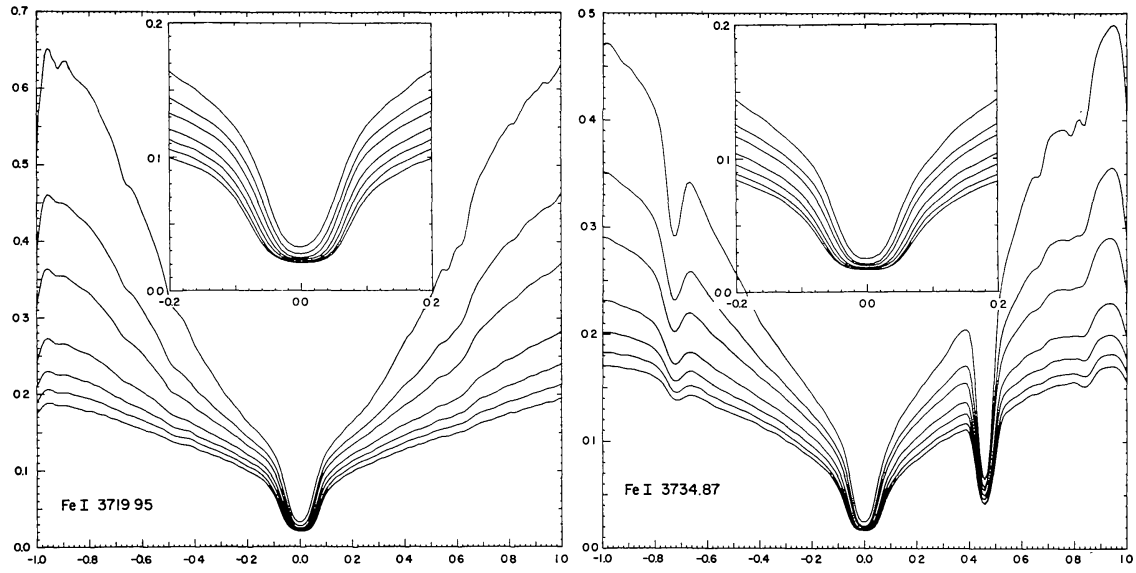

Fig. 1b. The limb darkening in the profiles of Fe I 3719.95 and Fe I 3734.87. Refer to Table I for the values of $\mu = \cos\theta$ for each profile.

we used the drift scan technique to measure the limb darkening at selected *drift scan windows* in the profile scans. The fifth column of Table I lists the wavelengths of the drift scan windows. These windows do not represent true continuum, even in the restricted sense of the Houtgast (1970) windows; they are simply bands included in the profile scans of high intensity and of minimum width 0.05 to 0.10 Å. The data gathering procedure for the drift scans differs markedly from the profile scan procedure. The drift scans were also taken with the spectrometer in the double pass mode since

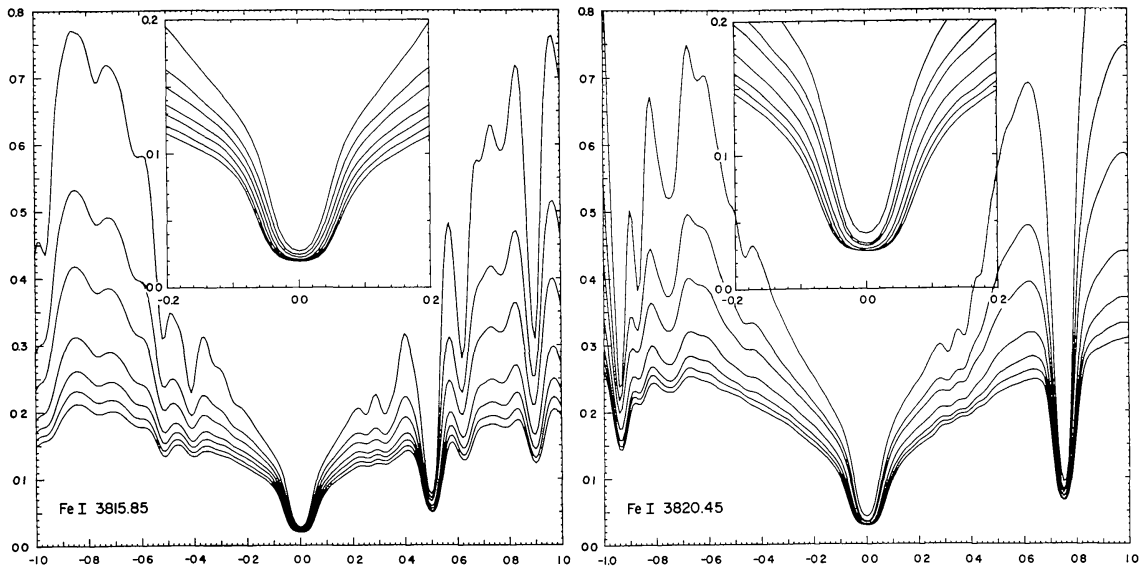

Fig. 1c. The limb in the line profiles of Fe I 3815.85 and Fe I 3020.45. Refer to Table I for the values of $\mu = \cos\theta$ for each profile.

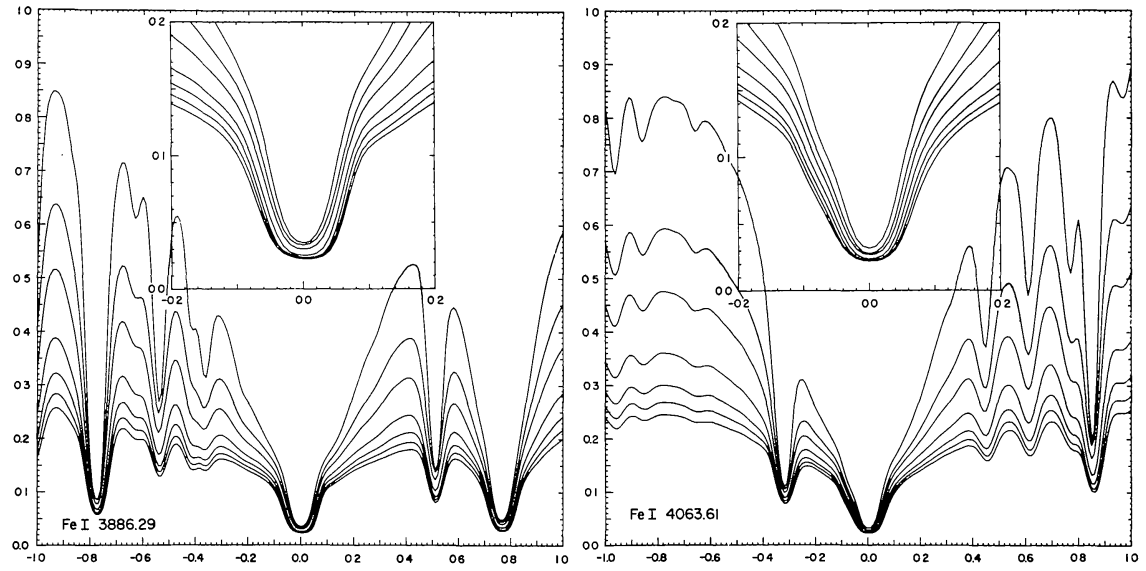

Fig. 1d. The limb darkening in the line profiles of Fe I 3886.29 and Fe I 4063.61. Refer to Table I for the values of $\mu = \cos\theta$ for each profile.

scattered light from other wavelengths may have a different limb darkening function. The limb darkening function was measured by digitizing the photometer output as the solar image was driven alternately north-south and south-north along a solar diameter. We accomplished the image scanning motion by running the tangent arm drive of the main heliostat mirror at its fastest rate. A scan required roughly 30 s of which 24 s were spent recording the limb darkening function between the two solar limbs. The data sampling rate of 200 points per second allowed the use of existing electronic data sampling filters to insure that the conditions of the sampling theorem were met; that is,

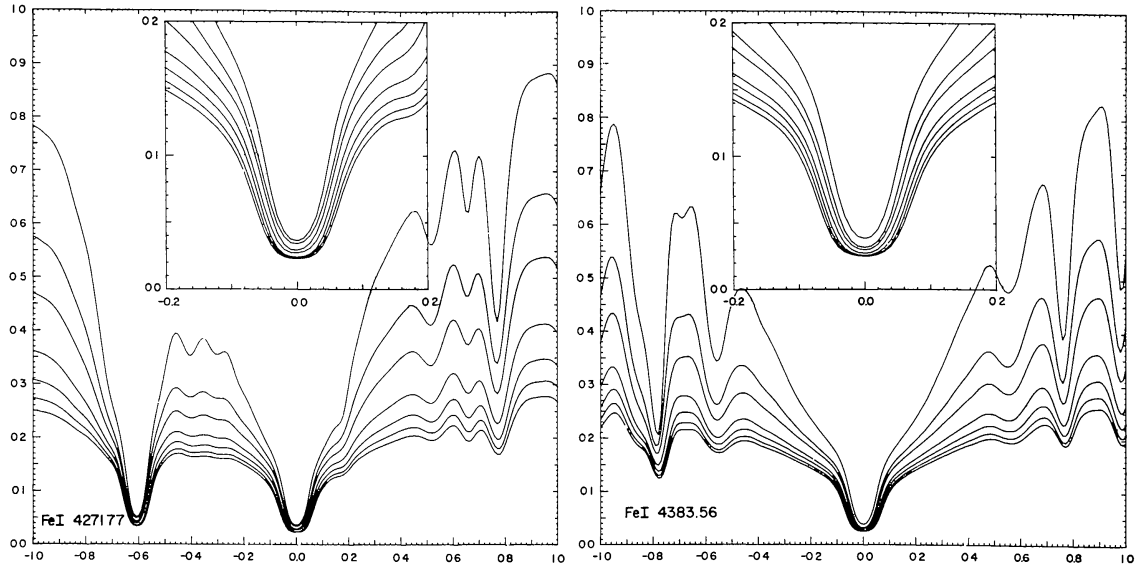

Fig. 1e. The limb darkening in the line profiles of Fe I 4271.77 and Fe I 4383.56. Refer to Table I for the values of $\mu = \cos\theta$ for each profile.

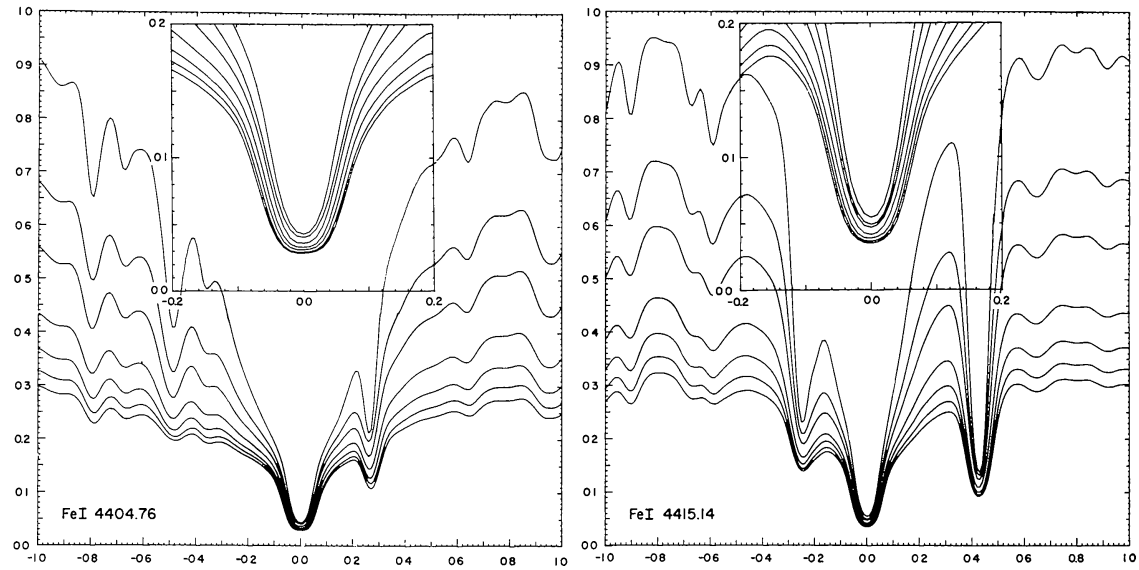

Fig. 1f. The limb darkening in the line profiles of Fe I 4404.76 and Fe I 4415.14. Refer to Table I for the values of $\mu = \cos\theta$ for each profile.

the measurement would not be contaminated by undersampled high frequency noise (see Brault and White, 1971).

B. MEASUREMENT OF THE LONG SCANS

The data collection procedure for the long scans is nearly identical to the procedure for the profile scans; the only differences occur in the number of points digitized and the number of scans averaged. In the sixth column of Table I we indicate the wavelength range of the long scans for each observed line. The wavelength spacing between each

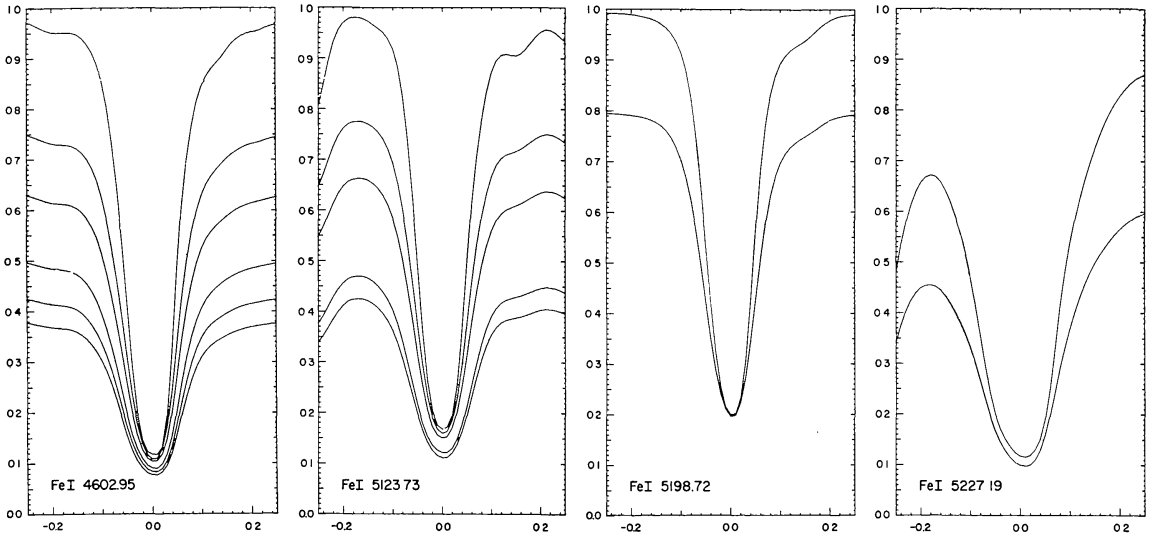

Fig. 1g. The limb darkening in the line profiles of Fe I 4602.95, Fe I 5123.73, Fe I 5198.72, and Fe I 5229.19. Refer to Table I for the values of $\mu = \cos\theta$ for each profile.

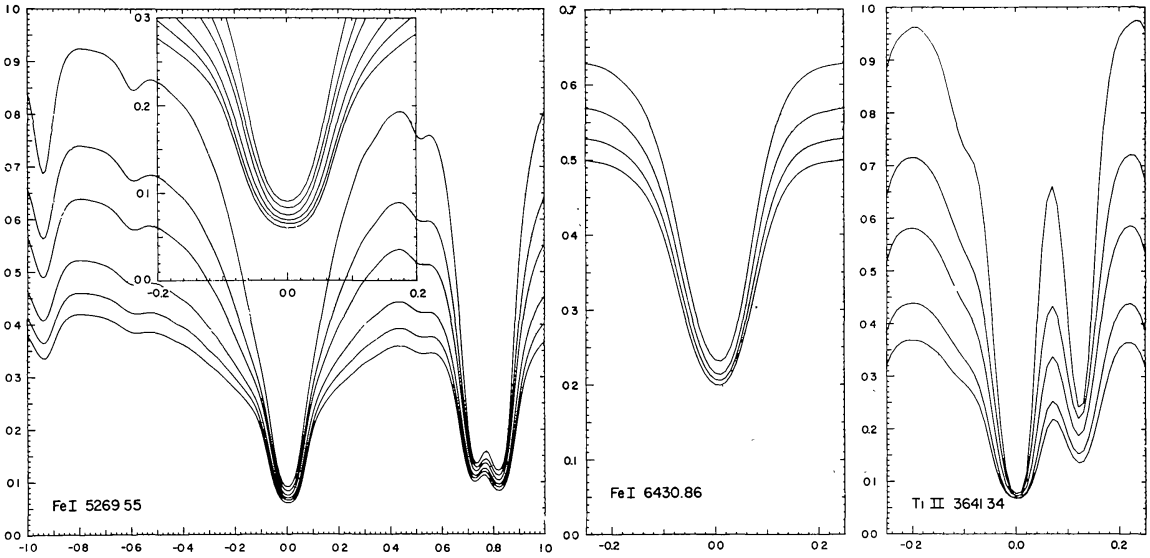

Fig. 1h. The limb darkening in the line profiles of Fe I 5269.55, Fe I 6430.86, and Ti II 3641.34. Refer to Table I for the values of $\mu = \cos\theta$ for each profile.

digitized point of a long scan is twice that of the corresponding profile scans, and 4096 points are digitized in each scan. The wavelength interval of the long scans is then four times that of the corresponding short scans. We relaxed the stringent profile scan requirement of freedom from statistical noise during measurement of the long scans and, as a result, the long scans required twenty minutes of telescope time but they only represent the average of 43 individual scans.

C. MEASUREMENT OF THE STANDARD LAMP SCANS

Both the long scans and the profile scans are affected by the slow wavelength variation

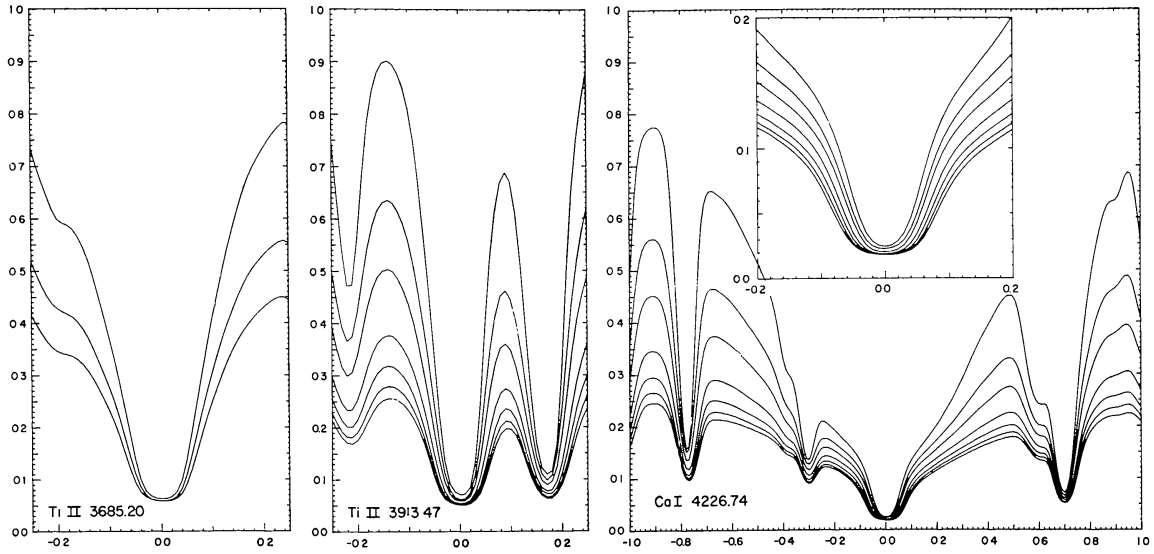

Fig. 1i. The limb darkening in the line profiles of Ti II 3685.20, Ti II 3913.47, and Ca I 4226.74. Refer to Table I for the values of $\mu = \cos\theta$ for each profile.

in the sensitivity of the spectrometer system. The grating blaze causes much of the sensitivity variation; however, the photocathode response, the wavelength dependence of the reflectance of mirrors on the spectrometer and predisperser, and the transmittance of the predisperser prism and order isolating filters also contribute. The largest effect of this spurious variation is upon the absolute intensity calibration because of the usual large wavelength separation of the observed lines and their corresponding absolute intensity reference windows.

The measurement of the wavelength variation in the sensitivity of the spectrometer system (including the predisperser) was accomplished by scanning the spectrum of a light source for which the absolute intensity is known as a function of wavelength. For this measurement the spectrometer system was adjusted as closely as possible to the corresponding long scan settings. Ideally these standard lamp scans should have been measured immediately preceding or immediately after both the long scans and the profile scans so as to insure a duplication of the instrument adjustments. The low intensity of the standard lamp in the near ultraviolet required a considerable integration time to reduce the statistical noise to an acceptable level; hence, the use of daylight observing time for this calibration measurement would have been prohibitive in view of the small corrections to the data involved. The standard lamp scans then took a secondary position in the observing priority and, hence, were made at night.

4. Numerical Processing of the Digitized Data

The numerical processing procedure for the collected data is intended to satisfy two primary objectives. The first of these objectives is to minimize the effects of errors introduced into the profile scans by the measurement process. The random noise present in the profile data, the smearing of the profile due to instrumental resolution, and the

TABLE II

The measured drift scan window intensities at the given μ-positions are shown in the first column of each entry, and the corresponding standard deviations σ of the measurements are given in the second column in percent of the relative intensities I_{rel}

	λ3439.428		λ3607.275		λ3718.537		λ3736.134		λ3818.916	
μ	I_{rel}	σ(%)	I_{rel}	σ(%)	I_{rel}	σ(%)	I_{rel}	σ(%)	I_{rel}	σ(%)
1.000	1.000	1.4	1.000	2.7	1.000	1.3	1.000	1.9	1.000	1.3
0.667	0.709	3.0	0.737	2.3	0.735	1.6	0.728	2.2	0.695	1.2
0.500	0.554	2.9	0.593	2.6	0.582	2.4	0.590	2.5	0.547	1.8
0.333	0.399	3.0	0.444	3.5	0.426	2.4	0.458	2.7	0.403	1.7
0.250	0.328	3.1	0.366	3.2	0.353	2.8	0.396	1.9	0.330	2.1
0.200	0.282	2.7	0.319	3.6	0.309	3.0	0.357	3.8	0.289	1.8
0.167	0.252	4.1	0.285	5.0	0.278	3.4	0.331	4.0	0.264	2.5
0.143	0.231	4.8	0.262	2.9	0.258	3.0	0.313	3.1	0.246	2.1
0.125	0.215	5.4	0.245	3.8	0.242	3.6	0.297	3.5	0.232	2.6
0.111	0.202	4.4	0.232	2.5	0.230	2.7	0.283	3.7	0.219	2.3
0.100	0.190	5.4	0.220	3.8	0.217	3.2	0.267	5.2	0.206	3.8

	λ3883.924		λ4064.847		λ4272,720		λ4382.340		λ4406.382	
μ	I_{rel}	σ(%)	I_{rel}	σ(%)	I_{rel}	σ(%)	I_{rel}	σ(%)	I_{rel}	σ(%)
1.000	1.000	0.91	1.000	1.4	1.000	0.82	1.000	0.50	1.000	0.74
0.667	0.760	1.2	0.726	0.95	0.738	1.0	0.740	1.0	0.755	1.2
0.500	0.621	2.0	0.586	1.8	0.600	1.3	0.604	0.92	0.623	0.99
0.333	0.471	2.0	0.443	2.1	0.461	1.4	0.465	1.4	0.485	1.2
0.250	0.390	1.9	0.365	1.5	0.389	1.3	0.397	1.1	0.412	1.1
0.200	0.340	2.8	0.322	2.2	0.346	2.1	0.353	1.4	0.366	0.95
0.167	0.304	1.6	0.289	2.7	0.314	1.4	0.321	1.2	0.332	1.4
0.143	0.279	2.6	0.290	1.8	0.292	1.8	0.302	1.4	0.309	1.2
0.125	0.259	1.7	0.255	2.0	0.275	1.7	0.286	1.4	0.292	1.3
0.111	0.242	2.7	0.242	2.6	0.262	1.8	0.271	1.7	0.277	1.5
0.100	0.228	3.1	0.229	2.3	0.250	1.6	0.257	1.8	0.263	1.8

	λ4417.106		λ5267.903		λ3640.830		λ3913.877		λ4228.892	
μ	I_{rel}	σ(%)	I_{rel}	σ(%)	I_{rel}	σ(%)	I_{rel}	σ(%)	I_{rel}	σ(%)
1.000	1.000	0.58	1.000	0.48	1.000	2.0	1.000	2.1	1.000	1.1
0.667	0.764	1.4	0.806	1.0	0.751	1.8	0.717	1.4	0.745	1.5
0.500	0.635	1.4	0.697	1.0	0.610	2.8	0.570	1.3	0.607	1.3
0.333	0.495	1.1	0.571	0.96	0.463	4.4	0.425	1.7	0.465	2.0
0.250	0.422	1.0	0.504	0.87	0.385	4.2	0.354	1.5	0.392	2.4
0.200	0.375	1.6	0.459	1.3	0.338	3.5	0.308	3.9	0.347	2.2
0.167	0.342	1.5	0.425	1.3	0.300	3.0	0.278	1.9	0.314	2.1
0.143	0.317	1.3	0.400	1.7	0.275	6.5	0.258	2.3	0.291	1.9
0.125	0.298	1.6	0.377	1.4	0.258	3.9	0.243	2.1	0.272	2.5
0.111	0.284	1.0	0.357	1.8	0.244	3.6	0.231	2.6	0.259	2.1
0.100	0.271	1.5	0.337	2.7	0.231	3.2	0.219	1.6	0.247	2.6

slowly varying sensitivity of the telescope and spectrometer may all be partially corrected for. The second objective of the numerical processing is to present the profile data in a form amenable to analysis from the standpoint of line profile synthesis. This entails relating the profile data to an absolute intensity scale by use of the drift scan data and the long scans, and definition of a common wavelength scale for the profile scans at each μ-position.

A. RESTORATION AND SMOOTHING OF THE PROFILE SCANS AND LONG SCANS

The vehicle used for most of this processing was an adaptation of the Kitt Peak National Observatory *Reducer* Computer code – a versatile computer program written to handle the reduction of the photometry data from the Kitt Peak solar spectrometer. This code employs the powerful 'fast Fourier transform' method (see Brault and White, 1971) for smoothing of the data and extraction of the instrumental broadening in a manner that preserves the basic information content of the observed spectra. The smoothing and restoration procedure used on the profile scan and long scan data is described in detail by Brault and White (1971).

B. NUMERICAL PROCESSING OF THE DRIFT SCAN DATA

The object of the drift scan data processing at each drift scan window λ was to extract the ratio $I_{\text{rel}}=I(\mu, \lambda)/I(1, \lambda)$ at all the μ-positions at which profile scans were made. This involved centering appropriately filtering the resultant average drift scan $I_{\text{av}}(\mu, \lambda)$ to obtain the relative intensities I_{rel}. This filtering procedure is carried out in the disk measurement coordinate $r=(1-\mu^2)^{1/2}$. The adopted filter function is simply the mean of the observed intensities $I_{\text{av}}(r, \lambda)$ in the range of disk positions $r(\mu)\pm A(r)$ centered on the disk position μ. The averaging width, $A(r)$, or the number of data points in the data points in the data record averaged to obtain I_{rel}, is a tradeoff between (a) the amount of random noise locally present at the disk position μ as determined from the data itself, and (b) the estimate of the local nonlinearity of the limb darkening function at (μ, λ) as given by Pierce and Waddell (1961). Table II lists the final relative intensities I_{rel} and the standard deviation σ of the random noise present in each limb darkening curve before filtering.

C. SMOOTHING THE STANDARD LAMP SCANS

A simple representation of the observed intensity versus wavelength is needed for the standard lamp data. Fourier transform techniques are not necessary to analyze the standard lamp data, so the scans were fitted with a quadratic function by a least squares procedure. The small curvature of the standard lamp scans did not require a more elaborate polynominal fit.

D. CENTERING THE PROFILE SCANS OF A GIVEN LINE: THE DEFINITION OF A WAVELENGTH SCALE

The *reducer* code includes a routine that accurately calculates the dispersion of a digitized spectrum scan given the spectrograph order and rough wavelength range,

however the user must supply an accurate reference wavelength within the scan to relate the scan to an absolute wavelength scale. Here we describe how the spectrum lines within the scan were used to define this reference wavelength.

An accurate absolute wavelength reference is necessary in each spectrum scan to locate the drift scan wavelength or absolute window wavelength, and it is also necessary to insure that normalization of the profile scans is applied at the same wavelength in scans at different μ-positions. In addition, the wavelength scale must serve to simultaneously center the scans at the various μ-positions of a given line. In this work we use only the Doppler core of the Fraunhofer line of interest in each profile scan and long scan to define the reference wavelength. We call this line the *primary line*. At first glance, the narrow lines included in a spectrum scan might seem to provide a more accurate wavelength reference than the (usually) broad primary lines. There are three reasons for the use of the primary lines instead of these narrower lines. First, the narrow lines are susceptible to observed asymmetry effects (de Jager and Neven, 1967). Second, these weaker lines are necessarily in the wings of the primary line in order to be included in the same profile scan, and hence the weaker lines may suffer from a large 'effective continuum' slope. The change in the wing of the strong line with position on the disk leads to an asymmetry in the weaker line which varies with disk position. Third, the use of the primary line of a profile scan insures a self-consistent,well-defined observational center to the line. The method we adopted to find line centers provides a wavelength scale yielding well-centered profiles for all observed lines in the strong to medium-strong category. Slight asymmetries occur in the narrowest lines observed.

The procedure for defining the wavelength reference is successfull because it uses the steep sides of the primary line Doppler core. The method is as follows: (a) find the minimum intensity of the primary line by a search of the core region, (b) find the wavelength regions of the steep sides of the Doppler core,(c) find the wavelength positions on the data point scale of 50 intensity levels equally spaced within the steep portions of the core, and (d) average the 100 positions of step c to obtain the observational center of the line.

E. CORRECTION FOR THE WAVELENGTH DEPENDENCE OF THE SPECTROMETER RESPONSE AND NORMALIZATION OF THE PROFILE DATA

The known intensity variation of the standard lamp, in conjunction with the standard lamp scans, allowed immediate correction of the profile scans and long scans for the slowly varying response of the spectrometer with wavelength. Once this correction had been made, it was only necessary to appropriately normalize the profile scans. The long scan measurements made possible the normalization of the disk center profile scans to unity at the respective *continuum windows*. The continuum window wavelengths are tabulated in the eighth column of Table I. Column 9 of Table I gives the absolute intensity of these continuum windows, and column 10 lists the source of the absolute intensity measurement: H for Houtgast (1970); LN for Labs and Neckel (1968). A further comment is in order here concerning the absolute intensity windows. Houtgast (1970) lists his instrumental resolving power at 10^5 and

as a result he only specifies his window wavelengths to the nearest 0.1 Å. We partially allowed for his lack of resolution by smearing the long scans at the wavelength of the continuum window, λ_0, with a Gaussian function of width $10^{-5}\ \lambda_0$. This smearing was also done for normalization with those long scans at wavelengths greater than 4100 Å where the Labs and Neckel (1968) intensities were used. Labs and Neckel give their absolute intensity calibration in terms of the 100% level of the Utrecht Photometric Atlas (Minnaert *et al.*, 1940). Intensities of the solar spectrum relative to this 100% level are necessarily subject to the resolving power of the spectrograph used for the Utrecht Photometric Atlas, which Minnaert *et al.* list at 1.5×10^5. Thus the wavelength averaging indicated above was effected over a slightly broader range than dictated by the Utrecht Atlas resolution and thus the Labs and Neckel (1968) absolute calibration. Above 4100 Å, the chosen continuum windows are considerably wider than many of the Houtgast windows, so this averaging does not grossly affect the normalization.

The profile scans at μ-positions away from disk center were then related to this continuum window normalization at disk center through the drift scan measurements. Suppose $D(\lambda_1)$ is the intensity of a disk center profile scan at its drift scan window, λ_1, relative to the intensity of the corresponding continuum window. The profile scans away from disk center were then normalized at λ_1 to the product $I_{\text{rel}} D(\lambda_1)$, where I_{rel} is given in Table II. Note that not all of the observed lines of Table I have drift scan data listed in Table II. In the limited observing time it was not possible to obtain drift scans for all the observed lines, so we adopted the limb darkening functions of Pierce and Waddell (1961) for the remainder of the lines. The seventh column of Table I indicates those lines with observed drift scans (DS) and those lines for which the Pierce and Waddell functions were used (PW). This step completes the numerical processing of the data.

5. Assessment of the Quality of the Measurements

In Table III we summarize the important sources of error remaining in the profile scans, and the sources of error in the auxiliary measurements that may affect the normalization of the profile scans. Where possible we have given the limits in the magnitude of the error source.

Estimates of the first three entries of the profile scan error result from the processing of the profile data in the Fourier transform domain. The first entry is an estimate of the low frequency random noise remaining in the profile scans after the smoothing of the data. The power spectrum of a signal due to random sources such as photon 'shot' noise or amplifier noise has a mean amplitude independent of the Fourier domain frequency s. We then estimate the mean amplitude of the white noise signal by integrating the mean noise power density over the bandpass of the optimum filter. The limits given in Table III for this source of error represent estimates from the profile scan with the least noise, $\lambda 5123$, $\mu = 1$, to the profile scan with fewest counted photons, $\lambda 3440$, $\mu = \frac{1}{6}$.

Other sources of noise in the profile scans are random but do not have characteristically flat power spectra. These sources are sometimes categorized as '$1/f$' noise

TABLE III

Summary of the important sources of error remaining in the profile scans, and the sources of error in the auxiliary measurements that may affect the normalization of them

Profile scans error source	Type of error	Probable magnitude (in % of local continuum, where applicable)
(1) Noise remaining after smoothing	Random	$>0.03\%$ $<0.2\%$
(2) '$1/f$' noise	Random	$\geqslant 0.2\%$ at $\mu = 1/10$ decr. rapidly with incr. μ
(3) Under-correction of profiles for instrumental broadening due to smoothing	Systematic	$>0.03\%$ $<0.2\%$
(4) Solar activity	Systematic	Probably negligible for $\mu \leqslant 1/2$
(5) Resonance polarization	Systematic	$<0.2\%$
(6) Smearing of profiles at limb due to seeing and image motion	Systematic	? (important only for $\mu \leqslant 1/6$)
Auxiliary measurements		
(1) Drift scan noise	Random	$\sim 0.2\%$ to 1% of disk center intensity
(2) Wavelength variation of telescope response and atmospheric transmittance	Systematic	$<2\%$ in absolute intensity calibration

sources since their power spectra very roughly as the inverse of the frequency. The majority of this type of noise present in the profile scans is probably due to image motion and seeing effects. The second entry in Table III concerns this type of noise. One of us (JWB) has developed a very useful data diagnostic technique that allows an estimation of the magnitude of this $1/f$ noise, and also permits evaluation of the general quality of a spectrum scan. This technique is part of the *Reducer* package. During acquisition, the individual spectrum scans are alternately stored in two separate channels so ideally the difference of these two channels should give a pure noise signal, even at the very low frequencies. This technique then allows direct measurement of the low frequency noise spectrum. Any problems with equipment or varying atmospheric conditions result in a clearly different character of the power spectrum of the difference of the two channels, even though these problems may not stand out in the scans themsleves.

Seeing cause $1/f$ noise through two mechanisms both connected with the steep gradient in the limb darkening curve near the limb. The first and most important arises from the limb guiders' failure to compensate for all the fluctuations of the limb position. The second arises from the variable mixing of radiation from different positions on the disk due to time-dependent blurring of the seeing itself. The estimate given in the second entry of Table III follows from an approximaton to the deviation of the difference

power spectrum of a scan from a flat, white noise spectrum. The particular profile scan chosen for this estimate was $\lambda 4383$, $\mu = \frac{1}{10}$; a scan taken during a period of good seeing. The contribution of seeing effects to the $1/f$ noise should be roughly proportional to the local slope of the limb darkening curve, so observations taken near the limb are most severely affected by this source of error. The $1/f$ noise becomes insignificant in nearly all cases for $\mu \leqslant \frac{1}{4}$.

Some of the high frequency components of the true solar power spectrum are lost during the smoothing process. The third entry in Table III is an estimation of this source of error: the undercorrection of the profiles for instrumental broadening. The optimum filter essentially finds the best tradeoff between noise remaining in the restored scan and the high frequency components of the true solar power spectrum lost during smoothing, so we have estimated this source of error to be comparable in magnitude to the white noise estimate of the first entry in Table III.

We call attention to some rather more elusive sources of error in the profile scans in entries 4, 5, and 6 in Table III. The upper limit placed upon the effects of resonance polarization on the profile scans are based upon the measurement of that effect in the core of the Ca I resonance line $\lambda 4226.7$ by Pecker (1971). From the first six entries in Table III we place the total error in the unnormalized profile scans at 0.5% of the continuum, at worst, within the range $1 \geqslant \mu \geqslant 0.2$. None of the profile scans would seem to be more accurate than 0.05% of the continuum intensity.

The uncertainties involved in the auxiliary measurements affect both the normalization of the profiles and the relative intensity scaling of the profiles between different μ-positions. These uncertainties are summarized in the last two entires of Table III. The error of the drift scan measurements after the filtering process will be roughly equal to σ listed in Table II divided by the square root of the number of points averaged. The number of points averaged at disk center is approximately 120; whereas, at $\mu = \frac{1}{10}$ the filter averages over only four points, so the reliability of the limb darkening function is roughly 0.1 σ at disk center and $\frac{1}{2}\sigma$ at $\mu = \frac{1}{10}$. The estimate of σ was carried out using data from both the north and south limbs, so the estimate includes a systematic error which might well be dominant: the asymmetry in the drift scans due to the uneven tangent arm drive rate. No attempt has been made to correct either the long scans or the profile scans for the wavelength variation in (1) the reflectance of the telescope mirrors, (2) the transmittance of the quartz image-integrating lens used during disk center spectrum scans, or (3) the transparency of the Earth's atmosphere. These unmeasured effects tend to be much smaller than the variations introduced by the grating blaze, and they affect only the normalization to the absolute intensity window. The last entry of Table III shows that, in the worst case, this correction would be of the order of two percent of the continuum intensity. This level of error is negligible in comparison with the accuracy of the absolute intensity measurements themselves.

6. Graphical Presentation of the Data

In the figures 1a–i we plot the line profiles data for all observed μ-positions $\mu \geqslant \frac{1}{6}$.

The strong line profiles are plotted on a two ångström interval centered on the observational line center, and the core regions of these strong lines are shown in greater detail in the inserts to these figures. These inserts give the line profiles over a 0.4 ångström range centered on the observational line center. The weaker lines are plotted only over a 0.5 Å range. All intensities in these figures are relative to the disk center intensities of the corresponding 'continuum windows' listed for each line in Table I.

With exception of the core region of some of the lines, all of the profiles darken toward the limb hence there is little ambiguity as to the association of the plotted profiles with the μ-positions listed in Table I. The core profiles of the strong lines show very little relative limb darkening near the limb, and hence may overlap at one or two μ-positions or become confused because of their proximity, and it is for this reason that the profiles have not been plotted for $\mu < \frac{1}{6}$. The amount of this overlap is well within the uncertainties in the observed profiles; and as demonstrated in Section 5 the major portion of this uncertainty is due to the lack of precision in the limb darkening curves at the drift scan windows. Therefore there exists a need for higher accuracy observations of the monochromatic limb darkening curves at reference wavelengths throughout the near ultraviolet solar spectrum, for example at the Houtgast (1970) windows.

Complete tables of these data are given in HAO Research Memo No. 185 which is available upon request from the High Altitude Observatory, P.O. Box 1470, Boulder, Col. 80302, U.S.A. These tables give intensities of the line profiles at 0.01 Å intervals for a two Angstrom band centered on the line centers, and normalized both to (a) the local continuum at $\mu = 1$ (as presented graphically here) and (b) the local continuum at each μ.

Acknowledgements

We are most grateful to Dr O. R. White for his frequent assistance and advice throughout all phases of this work. We also thank the staff of the Kitt Peak National Observatory, especially Dr A. K. Pierce, R. W. Aikens, and C. D. Slaughter, for continued assistance during the observational phase of this study. The staff of the computing facility at the National Center for Atmospheric Research are to be commended for their efficient and helpful operation. We also thank Mrs Ruby Fulk for patiently typing several drafts of the manuscript. Finally, this extensive observing program would not have been possible without the generous grant of observing time at Kitt Peak provided by the Association of Universities for Research in Astronomy.

References

Athay, R. G., Brault, J. W., Lites, B. W., and White, O. R.: 1972, *Solar Phys.* **24**, 18.
Brault, J. W. and White, O. R.: 1971, *Astron. Astrophys.* **13**, 169.
Brault, J. W., Slaughter, C. D., Pierce, A. K., and Aikens, R. S.: 1971, *Solar Phys.* **18**, 366.
De Jager, C. and Neven, L.: 1967, *Solar Phys.* **1**, 27.
Houtgast, J.: 1970, *Solar Phys.* **15**, 273.
Labs, D. and Neckel, H.: 1968, *Z. Astrophys.* **69**, 1.
Lites, B. W.: 1972, *Observation and Analysis of the Solar Neutral Iron Spectrum*, Ph.D. Thesis, University of Colorado.

Minnaert, M., Mulders, G. F. W., and Houtgast, J.: 1940, *Photometric Atlas of the Solar Spectrum from 3613 to 8771 Å*, Schnabel, Kampert und Helm, Amsterdam.
Pecker, J.-C.: 1971, private communication.
Pierce, A. K. and Wandell, J. H.: 1961, *Mem. Roy. Astron. Soc.* **67**, 89.
Tanaka, K.: 1971a, *Publ. Astron. Soc. Japan* **23**, 185.
Tanaka, K.: 1971b, *Publ. Astron. Soc. Japan* **23**, 217.